Compact, Highly Efficient, and Fully Flexible Circularly Polarized Antenna Enabled by Silver Nanowires for Wireless Body-Area Networks

Zhi Hao Jiang, *Member, IEEE*, Zheng Cui, Taiwei Yue, *Student Member, IEEE*, Yong Zhu, and Douglas H. Werner, *Fellow, IEEE*

***Abstract*—A compact and flexible circularly polarized (CP) wearable antenna is introduced for wireless body-area network systems at the 2.4 GHz industrial, scientific, and medical (ISM) band, which is implemented by employing a low-loss composite of polydimethylsiloxane (PDMS) and silver nanowires (AgNWs). The circularly polarized radiation is enabled by placing a planar linearly polarized loop monopole above a finite anisotropic artificial ground plane. By truncating the anisotropic artificial ground plane to contain only 2 by 2 unit cells, an integrated antenna with a compact form factor of $0.41\lambda_0 \times 0.41\lambda_0 \times 0.045\lambda_0$ is obtained, all while possessing an improved angular coverage of CP radiation. A flexible prototype was fabricated and characterized, experimentally achieving $S_{11} < -$ 15 dB, an axial ratio of less than 3 dB, a gain of around 5.2 dBi, and a wide CP angular coverage in the targeted ISM band. Furthermore, this antenna is compared to a conventional CP patch antenna of the same physical size, which is also comprised of the same PDMS and AgNW composite. The results of this comparison reveal that the proposed antenna has much more stable performance under bending and human body loading, as well as a lower specific absorption rate. In all, the demonstrated wearable antenna offers a compact, flexible, and robust solution which makes it a strong candidate for future integration into body-area networks that require efficient off-body communications.**

***Index Terms*—Off-body communications, polydimethylsiloxane (PDMS), silver nanowires (AgNWs), wearable antenna, wireless body-area networks.**

I. Introduction

As THE technologies of wireless body-area networks (WBANs) and wearable electronics devices continue to develop at a rapid pace, the demand for compact high-performance flexible wearable antennas has dramatically increased, particularly those capable of supporting efficient off-body communications [1]–[4]. Wearable antennas share many of the same requirements as conventional antennas, such as impedance bandwidth, radiation patterns, gain, polarization, etc. However, it is also desirable that wearable antennas are well isolated from loading effects when placed in close proximity to the human body, while simultaneously having the smallest possible thickness and lateral footprint [5], [6]. In such a way, the wearable antenna can still transmit/receive signals with a high operating efficiency, and at the same time the exposure of the human body to electromagnetic radiation, characterized by the specific absorption rate (SAR), remains well within the margin of safety. Apart from the structural designs of wearable antennas, recent advancements in material science and engineering have brought about new possibilities of high-quality flexible conducting and dielectric materials in the microwave/RF frequency range, thereby providing a broader choice of constitutive materials for microwave circuits [7], [8] and antennas [9]–[12]. As a result, various soft materials have been employed as low loss antenna substrate as well as conducting layers, which have enabled some of the first truly flexible wearable antennas.

So far, several off-body communication antennas, with and without the integration of flexible materials, have been proposed for wearable applications in the 2.4 GHz industrial, scientific, and medical (ISM) band. Apart from monopoles [5], [13], conventional patch antennas [14], and slot antennas [15], which were considered at the early stages of wearable antenna development, more versatile and advanced antenna designs with enhanced performance and multiple functionalities have been introduced and demonstrated over the past several years. Particularly, substrate integrated waveguide fed slot antennas have been realized using textile materials, exhibiting either single- or dual-band operation [16]–[18]. Meanwhile, broadband inverted-F textile antennas [19], [20] and multi-band embroidered planar monopole antennas [21] have also been reported, which possess a small footprint but may lead to higher SAR values when operating at extreme close proximity to human body surfaces due to their nearly bi-directional radiation patterns. In an effort to minimize the impact of human body loading and improve the isolation, artificial ground planes with isotropic unit cells have been introduced and implemented using textile materials [22]

Manuscript received December 21, 2016; revised February 13, 2017; accepted February 15, 2017. Date of publication May 23, 2017; date of current version July 26, 2017. This work was supported by the National Science Foundation ASSIST Nanosystems ERC under Award Number EEC-1160483. This paper was recommended by Associate Editor P. Mercier.

Z. H. Jiang was with the Electrical Engineering Department, The Pennsylvania State University, University Park, PA 16802 USA. He is now with the State Key Laboratory of Millimeter Waves, Southeast University, Nanjing 210096, China (e-mail: zhihao.jiang@seu.edu.cn).

Z. Cui and Y. Zhu are with the Department of Mechanical and Aerospace Engineering, North Carolina State University, Raleigh, NC 27695 USA (e-mail: zcui@ncsu.edu; yzhu7@ncsu.edu).

T. Yue and D. H. Werner are with the Electrical Engineering Department, The Pennsylvania State University, University Park, PA 16802 USA (e-mail: txy143@psu.edu; dhw@psu.edu).

Color versions of one or more of the figures in this paper are available online at http://ieeexplore.ieee.org.

Digital Object Identifier 10.1109/TBCAS.2017.2671841

1932-4545 © 2017 IEEE. Personal use is permitted, but republication/redistribution requires IEEE permission.
See http://www.ieee.org/publications_standards/publications/rights/index.html for more information.

as well as with polymer and printed silver ink [23]. Such textile-based isotropic artificial ground planes have also been used to provide dual-band operation, which behave as a perfect electric conducting ground at the patch mode frequency and as a perfect magnetic conducting ground at the dipole mode frequency [24]. More recently, an anisotropic artificial ground plane containing I-shaped resonating unit cells was employed to achieve a high degree of antenna-to-body isolation with a much smaller antenna footprint [25].

It should be emphasized, however, that almost all of these wearable antennas are linearly polarized (LP), which could result in unreliable wireless links due to possible complete polarization mismatch caused by the constant human body motion expected under realistic scenarios. Circularly polarized (CP) antennas, in contrast, tend to be more favorable for wearable applications due to their improved signal robustness with respect to human body movement. Surprisingly, there has been a very limited amount of work reported on CP wearable antennas. It has been shown that coplanar waveguide fed planar slot monopoles can generate wideband CP radiation [26]. However, due to their bi-directional radiation pattern, a significant amount of energy is absorbed by the human tissue, making them unsuitable for operation in close proximity to a human body. The pin-fed and microstrip-fed textile CP patch antennas with truncated corners produce unidirectional radiation [27], [28]. However, the overall footprint of these antennas is rather large, which is primarily attributed to a large ground plane required for sufficient shielding and the low permittivity value of the textile material employed in the substrate. Such a large overall footprint causes the antenna to suffer from significant frequency shift due to structural deformation. Recently, a design methodology was introduced where microwave circuits could be seamlessly integrated into the antenna design. This technique enables integrated wearable modules with simultaneous band-pass filtering and CP radiation functionalities [29], [30], at the expense of requiring that vertical vias be embedded into the structures. Miniaturization techniques such as introducing various types of slots at the center [31], [32] or on the edges [33] of the patch radiator enables a more compact footprint and less resonance shift due to bending. Nevertheless, the reduced cavity volume greatly increases the quality factor of the resonance, resulting in a narrower impedance and axial ratio (AR) bandwidth and/or a lower gain/efficiency. Therefore, a flexible CP antenna simultaneously possessing a robust performance, a compact form factor, a high efficiency, and a reasonably wide bandwidth is highly desirable for wireless BAN systems.

In this paper, we demonstrate a flexible and compact CP antenna implemented using a polydimethylsiloxane (PDMS) and silver nanowire (AgNW) composite material system for wearable applications in the 2.4 GHz ISM band. Section II describes the antenna design and presents a study of the truncation effects of the anisotropic artificial ground (AAG). In Section III, the fabrication process and measured results of the proposed antenna are reported. Its performance is compared to a reference prototype of the same antenna design but implemented by using conventional printed circuit board (PCB) technology with rigid substrate material and copper. Section IV discusses the comparison among the proposed antenna, a conventional CP patch antenna, and a miniaturized CP patch antenna, a demonstrating its superior and more robust performance under structural deformation. In Section V, the effects of human body loading on the performance of the proposed antenna under various scenarios, including the antenna's electrical properties and the specific absorption rate (SAR), are investigated and compared to its conventional CP patch antenna counterpart.

II. Antenna Configuration and Design

A. Flexible Constitutive Material System

The majority of the previously reported work on flexible antenna designs involves replacing conventional substrates with textile or fabric materials. Here we report on a new type of flexible material system for wearable antenna integration that is based on a PDMS and AgNW composite. PDMS is a widely used elastomer with a high stretchability. It has a reported relative permittivity (ε_r) that ranges from 2.67 to 3.0 with a corresponding loss tangent (tan δ) that varies between 0.01 and 0.05 over the frequency range of 1.0 to 5.0 GHz [34], [35]. A split-post dielectric resonator method [36] was used to characterize the in-house fabricated PDMS films, which consistently predicts a dielectric property with $\varepsilon_r = 2.8$ and tan $\delta = 0.02$. The dielectric constant of the PDMS is significantly higher than most previously employed textile and fabric type of substrate materials [16]–[24], [26]–[28], [31]–[33], which makes it ideal for use in the design of compact flexible antennas. Moreover, the PDMS/AgNW composite can be optimized to yield a highly conductive material ($\sim$8130 S cm^{-1}) [37]. By embedding a high-density mixture of AgNWs into a PDMS matrix makes possible the inclusion of a separate PDMS/AgNW conducting layer into the host PDMS substrate. Importantly, the thickness of both conducting and insulating layers can be well controlled. In this work, the thickness of the conducting layer is fixed at around 0.1 mm, which provides a reasonable compromise between conductivity homogeneity and mechanical flexibility, while the thickness of the insulating layers can vary between 0.5 and 5 mm. The general polymer/AgNW composite material system represents a promising technology for developing flexible and stretchable electrodes, which can be applied to light emitting diodes [38], solar cells [39], touch sensors [40], [41], wearable sensors [42], electrophysiological electrodes [35] and antennas [43], [44]. It should be noted that, in contrast to many thin plastic materials which are flexible but not compliant, the PDMS material is not only flexible but also compliant, making it an ideal candidate to form conformal and comfortable contact with the human skin.

B. Antenna Configuration

The layout of the compact and flexible CP wearable antenna is illustrated in Fig. 1(a), where a fully planar configuration is adopted. The antenna consists of two components separated by a thin foam spacer–a planar ring monopole oriented along the *x*-direction on the top and a custom designed AAG on the bottom. The side-fed scheme allows the antenna to be placed

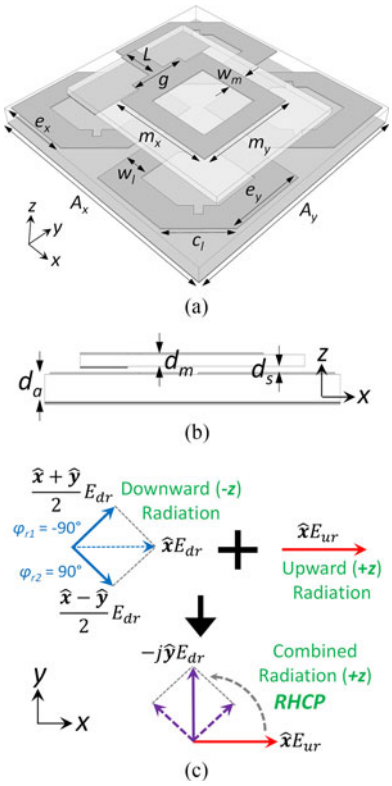

Fig. 1. (a) 3D view and (b) side view of the proposed CP antenna. The optimized dimensions are $A_x = 50, A_y = 50, m_x = 21, m_y = 21, w_m = 4, g = 12, L = 8, e_x = 15, e_y = 15, c_l = 11.6, w_l = 5, d_a = 3.5, d_s = 0.5$, and $d_m = 1.5$, all in millimeters. (c) Illustration of the field decomposition and combination required for generating a RHCP radiated wave at broadside.

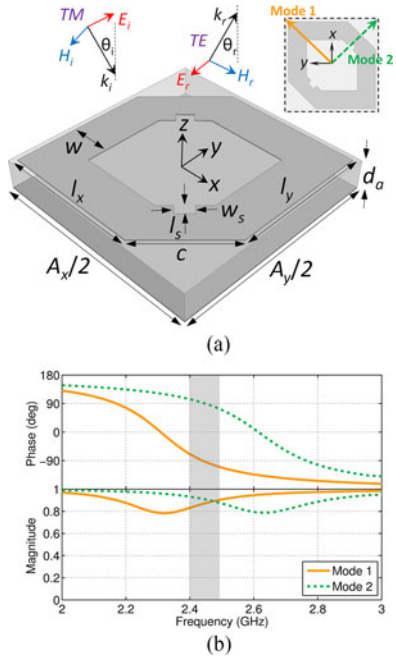

Fig. 2. (a) 3D view of the AAG unit cell. The illuminating TM polarized plane wave is transformed into a TE polarized reflected wave. The dimensions are $w = 5, l_x = 16.5, l_y = 16.5, c = 10.2, w_s = 2, l_s = 1.5$, and $d_a = 3.5$, all in millimeters. The inset defines the modes along the mirror symmetry lines of the MLR. (b) Reflection magnitudes and phases of a normally incident plane wave for the two modes.

in very close proximity to the human body surface as compared to the bottom-fed topologies that have been considered in previous CP wearable patch antennas [27], [31], [32]. Artificial ground structures have been previously used in wearable antenna designs for both off-body [22]–[25] and on-body [45] communications, achieving a more compact antenna footprint and an improved degree of isolation. But these antennas were limited to designs that radiate only linearly-polarized waves. In contrast to a conventional ground plane, here the AAG contains a highly-truncated metasurface comprised of only a 2 by 2 array of modified loop resonators (MLRs) backed by a continuous conducting sheet. The MLR design was inspired by previous studies on isotropic artificial ground unit cells, which revealed that the loop resonator possesses a superior performance compared to cross-dipole or patch resonators [46]–[50]. In order to create the required anisotropic response, each MLR includes a pair of diagonal chamfered corners along with a pair of slots cut out from its interior. As has been reported, when an x-polarized LP source is radiating above an artificial ground with an anisotropic reflection phase response, in general, the polarization of the resulting wave is elliptical (*i.e.*, the wave directly radiated from the source antenna combined with that reflected from the AAG). To support right-handed (RH) CP radiation, as illustrated in Fig. 1(c), the reflection phases along the $x + y$ and $x - y$ directions must be around $-90°$ and $+90°$, respectively, while at the same time the reflection magnitudes in the two directions should be similar to each other. In this particular case, the reflected wave of the x-polarized downward radiation from the source then becomes y-polarized with a 90° phase delay, thus enabling a RHCP radiated wave at broadside when it is combined with the x-polarized upward radiation directly from the source [51], [52].

C. Unit Cell Design

The first step in the antenna design process is to consider the anisotropic reflection phase response of the AAG unit cell in an infinite array environment with a periodic boundary condition and Floquet port setup in the high frequency structure simulator (HFSS) [53]. As the inset of Fig. 2(a) shows, the MLR has its symmetry lines along the $x + y$ and $x - y$ directions, thereby two orthogonal resonating modes can be identified, denoted as Mode 1 and Mode 2, respectively. For a normally incident plane wave with its electric field polarized along these two directions, the reflection magnitudes and phases are different. Basically, the edge length, width, and slot size of the MLR as well as the capacitive coupling between adjacent MLRs determine the resonant frequency of Mode 1. The degree to which the resonant frequency of Mode 2 differs from Mode 1 is controlled by the chamfered corners. As shown in Fig. 2(b), the reflection phase for Mode 1 is around $-90°$ in the targeted band, while for Mode 2 it is in the vicinity of $+90°$. In addition, the reflection magnitudes have similar values of about 0.9. It is important to note that if the operational band is located in between the two resonances, lower absorption loss can be achieved, thus ensuring a high efficiency for the flexible antenna.

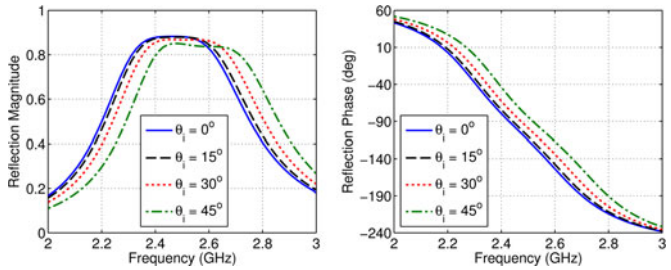

Fig. 3. Magnitude and phase for a TE polarized reflected wave with a TM polarized incident wave at different angles of incidence.

The majority of the downward radiated waves emanating from the planar monopole will impinge on the AAG at angles close to normal incidence. However, since the distance between the two components is on a deep subwavelength scale, there also exists waves with a non-zero transverse wavenumber, *i.e.* waves that obliquely illuminate the AAG. Thus, the angular response of the AAG needs to be taken into account. For oblique incidence angles, the requirement of the AAG is to transform a transverse magnetic (TM) polarized incident wave into a transverse electric (TE) polarized wave with its electric field polarized along the y-direction with a 90° phase delay. It can be observed from Fig. 3 that, in the targeted band, the magnitude and phase of the TE polarized reflected wave is larger than 0.84 and around $-90°$, respectively. The ratio between the power of the reflected TE and TM polarized wave is more than 13 dB, indicating that the TM polarized incident wave is almost entirely transformed into a TE polarized reflected wave within a certain field-of-view. This makes possible a wide axial ratio $<$3 dB beamwidth (ARBW), as will be shown in the following sections.

D. Integrated Antenna Design and Performance

Once the AAG unit cell has been designed, a planar monopole is added above the AAG structure with a separation distance of d_s. Since a strongly truncated AAG with only 2 by 2 unit cells is chosen in order to obtain a compact footprint, the radiating element of the monopole is located above the area in the middle of the four MLRs. In order to excite the four MLRs more efficiently, a rectangular loop monopole was employed which forces the currents to flow at locations near the corners of all four MLRs. Due to the truncation of the AAG, the dimensions of the MLRs need to be slightly tuned together with the planar loop monopole for the best performance metric in the targeted band, including the input impedance, gain, front-to-back total radiation (FBTR) ratio, AR bandwidth and beamwidth. Here, the FBTR ratio is defined as the ratio between the total radiated power in the half-space above the antenna and that in the half-space beneath the antenna. This represents a more meaningful characterization of the back radiation of an antenna towards the human body in wearable scenarios than the conventional front-to-back (FB) ratio.

The final tuned version of the integrated antenna has a form factor of $0.41\ \lambda_0 \times 0.41\ \lambda_0 \times 0.045\ \lambda_0$, where λ_0 is the wavelength at the center frequency of 2.44 GHz. The simulated S_{11}, shown in Fig. 4(a), has a -10 dB bandwidth that ranges from

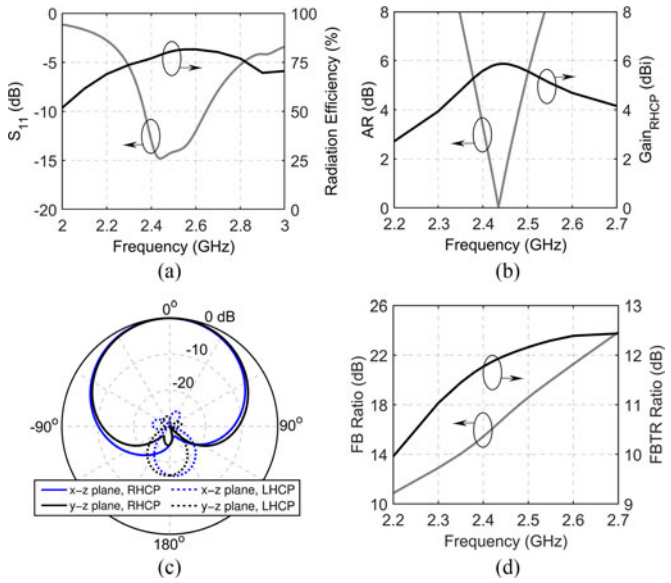

Fig. 4. Simulated (a) S_{11}, radiation efficiency, (b) broadside AR, and RHCP gain of the proposed antenna. (c) Simulated normalized RHCP and LHCP radiation patterns in the x-z and y-z planes at 2.44 GHz. (d) Simulated FB ratio and FBTR ratio of the proposed antenna.

2.37 to 2.64 GHz. It is below -14 dB in the targeted ISM band. The broadside AR is centered at 2.44 GHz, with an AR $<$3 dB bandwidth of 69 MHz. As presented in Fig. 4(b), the simulated gain for the RHCP radiated wave is higher than 5.6 dBi with a maximum value of 5.9 dBi, indicating a radiation efficiency of around 76–79% in the targeted band [see Fig. 4(a)]. The normalized simulated patterns for both the RHCP and LHCP radiated waves in the x-z and y-z planes are shown in Fig. 4(c), which exhibit a symmetric main beam with a half power beamwidth (HPBW) of 88.5° and 88.8° in the two planes, respectively. The strength of the LHCP radiated wave is significantly smaller than that of the RHCP wave over a wide angular range, implying the proposed antenna possesses a broad AR $<$ 3dB beamwidth. The radiation towards the half-space below the antenna is significantly smaller than that in the upper half-space, which is desired for wearable applications. As plotted in Fig. 4(d), the FB ratio is about 16 dB in the targeted band, while the FBTR ratio is around 12 dB, indicating that the total radiated power towards the half-space below the antenna is less than 6%.

E. Truncation Effects of AAG and Ground Plane

In this section the truncation effects of the AAG as well as the ground plane on the performance of the antenna are studied. To this end, we consider antennas with 4×4 MLRs, 3×3 MLRs, 2×3 MLRs and 3×2 MLRs comprising the AAG (as depicted in Fig. 5), and compare their performance to the proposed antenna that has an AAG with only a 2×2 array of MLRs. As shown in Fig. 6(a), all five antennas exhibit good impedance matching in the targeted band. Interestingly, a broadband response can be observed for the antennas with 3 MLRs along the x-direction. This can be attributed to the fact that the monopole radiator and the MLRs in the middle row

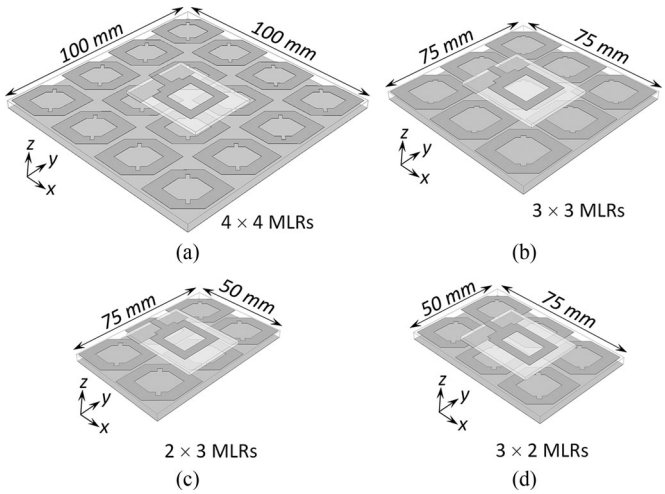

Fig. 5. Four antennas with (a) 4×4, (b) 3×3, (c) 2×3, and (d) 3×2 MLRs in the truncated AAG.

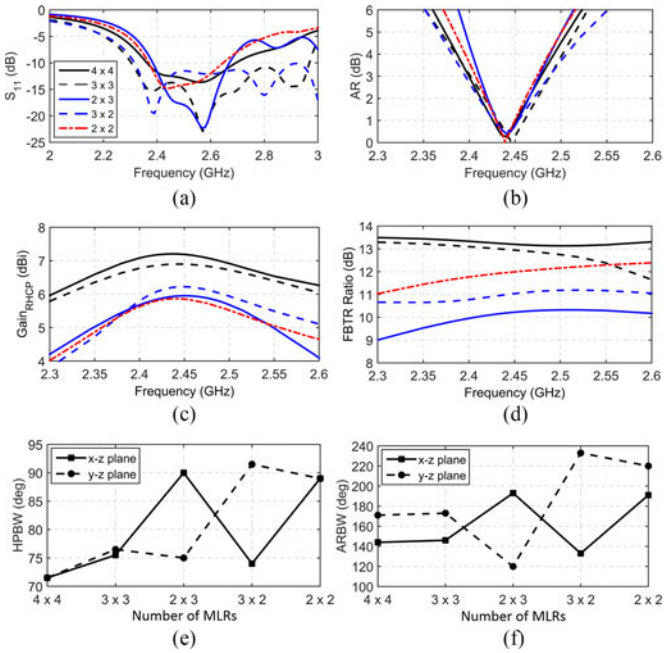

Fig. 6. The simulated (a) S_{11}, (b) broadside AR, (c) RHCP gain, and (d) FBTR ratio of the five antennas with different numbers of MLRs in the AAG. Simulated (e) HPBW and (f) ARBW of the five antennas at 2.44 GHz, *i.e.* the frequency at which the AR is minimum.

have no staggering along the *x*-direction, while in contrast a staggering of a half period exists for the cases where there is an even number of MLRs along the *x*-direction. Such a dramatic variation in the S_{11} response is ascribed to the different near-field coupling between the monopole and the truncated AAG, which corroborates findings in previously reported works [47], [54]. However, as seen from Fig. 6(b), the differences in the broadside AR response is less significant among the five antennas since the formation of the CP radiated waves is primarily determined by the anisotropic reflection phase property of the AAG. It is noted that the antennas with 3 MLRs along the *x*-direction have a slightly broader AR $<$ 3 dB bandwidth, which is around 90 MHz. For the other three antennas, however, which have an even number of MRLs comprising the AAG, the AR $<$ 3 dB bandwidth ranges from 67 to 76 MHz. In terms of gain, Fig. 6(c) shows that a larger footprint yields a higher antenna gain since the aperture, which is filled by the MLRs, becomes larger. Nevertheless, all these antennas have a similar radiation efficiency. The antennas that contain a 3×3 and 4×4 array of MLRs have a gain value of only 1 dB and 1.3 dB higher than that of the proposed antenna, respectively. However, this comes at the expense of a greatly increased antenna footprint of 225% and 400% in the two cases. This indicates that the marginal gain enhancement drops very quickly when the number of MLRs in the AAG is increased. It is also seen that the proposed antenna, which has a 2×2 array of MLRs, yields a similar gain to the antennas having a 2×3 and a 3×2 array of MLRs. Remarkably, the antenna with the 2×2 array of MLRs has a higher FBTR ratio than either the antenna with the 2×3 array or the 3×2 array of MLRs, even though the footprints of the latter two are 50% larger. This is due to the fact that an AAG with the same number of MLRs in the *x*- and *y*-directions results in a more symmetrically radiated beam as well as edge diffractions in the *x*-*z* and *y*-*z* planes, thereby reducing the amount of power diffracted into the half-space below the antenna. Such symmetrically radiated beams are also manifested in the HPBW and ARBW in both the *x*-*z* and *y*-*z* planes. As presented in Fig. 6(e) and (f), it can be seen that the proposed design with a 2×2 array of MLRs has the widest HPBW and ARBW. In all, this study shows that the antenna design containing the AAG with a 2×2 array of MLRs has the most suitable properties for wearable applications, *i.e.* the smallest footprint with a wide angular coverage of circular polarization and radiated power.

In order to investigate the impact of edge diffraction caused by the compact-sized ground plane on the performance of the proposed antenna, several different ground plane sizes were considered with the number of MLRs in the AAG fixed at 2 by 2. As can be seen from Fig. 7(a), the $S_{11} < -10$ dB and AR $<$ 3 dB bandwidths are both well maintained as the size of the ground plane increases. Fig. 7(b) shows that a fluctuation of less than 1.4 dB can be observed in the peak gain when the ground plane size is increased from 50 mm to 300 mm, *i.e.* $\sim 2.5\lambda_0$, which is smaller than that for conventional patch antennas [55], [56]. Importantly, the maximum gain value, which occurs when the ground plane size is 125 mm by 125 mm, is only 1.1 dB higher than the proposed case, but at the expense of a greatly increased footprint. The radiation efficiency is well-maintained to be above 77%. In fact, a smaller ground plane size is preferable since a larger ground plane requires more AgNW material which would result in increased Ohmic loss. In all, the ground plane size has a very minor effect on the performance of the antenna.

III. Fabrication and Measurements

The top planar monopole and the bottom AAG were fabricated separately and then assembled together. The first step in the fabricated process was to prepare liquid PDMS by mixing two parts of Sylgard 184 (Dow Corning) at a ratio of 10:1. Liquid PDMS was spin-coated on a cleaned Si wafer at 250 r/min

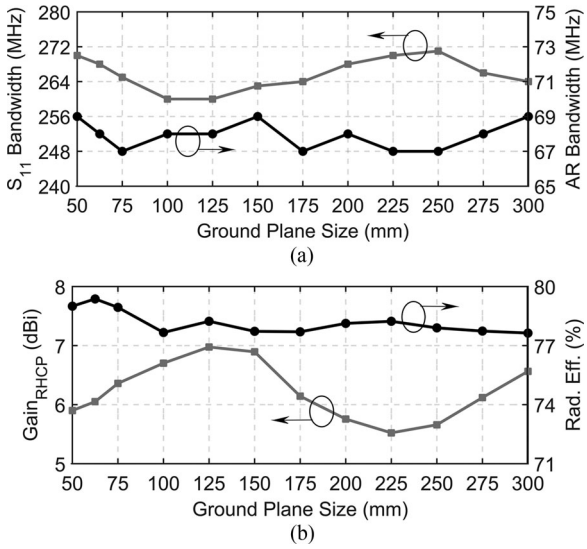

Fig. 7. The simulated (a) $S_{11} < -10$ dB bandwidth and AR < 3 dB bandwidth, and (b) RHCP gain and radiation efficiency as a function of the ground plane size.

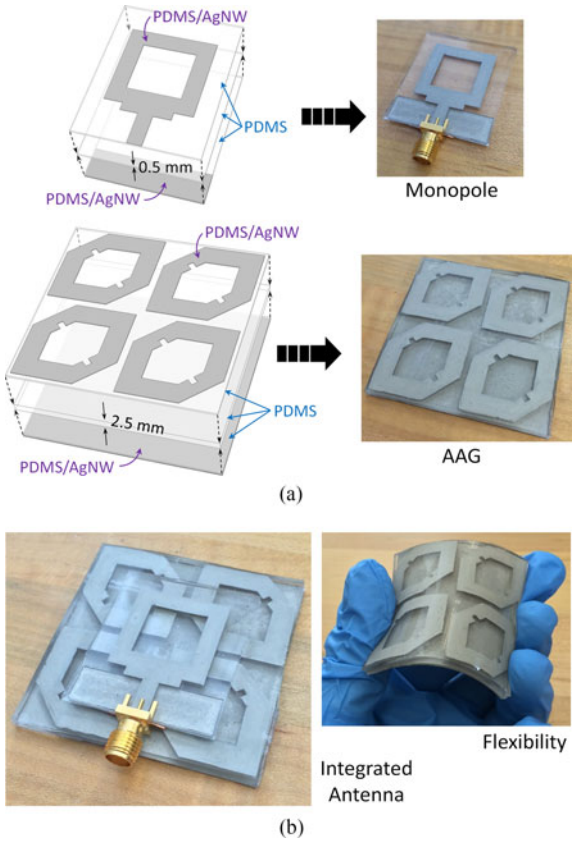

Fig. 8. (a) Fabrication process and photographs of the monopole and the AAG components. (b) Photographs of the integrated antenna prototype demonstrating flexibility.

for ∼2 min followed by curing in a degassed oven for 20 min at 70°C. As such, a thin layer of PDMS (∼300 μm) was obtained. Then, AgNWs with a diameter of around 60 nm and a length of about 30 μm were synthesized and diluted in ethanol with a concentration of 10 mg/ml. The patterns for the four different conducting layers of the proposed antenna were cut out on the cured PDMS to create PDMS masks. In the following step, the AgNW solution was drop casted into the grooves of the mask and dried at 55°C, thereby forming the conductive AgNW patterns as desired. Then the PDMS mask was peeled off and the AgNW pattern was coated with another layer of liquid PDMS with a thickness of ∼0.5 mm, followed by a curing process. Next, the patterned AgNW/PDMS films were cut out to have the designed form factors and stacked together with cured bare PDMS layers of 0.5 mm and 2.5 mm to form the top monopole and bottom AAG components, respectively, as illustrated in Fig. 8(a). Finally, a foam spacer with the prescribed thickness was added in between the two components to form the final integrated CP wearable antenna prototype, which is fully planar and highly flexible [see Fig. 8(b)].

An Agilent E8364B network analyzer was used to characterize the S_{11} of the fabricated antenna. As shown in Fig. 9(a), good agreement was obtained between simulated and measured results. The S_{11} is below -15 dB in the targeted band. The broadside AR is smaller than 3 dB within a 67 MHz band centered at 2.46 GHz, which has a <1% shift from the simulation prediction. The simulated and measured gain patterns of the total radiated power at the frequency corresponding to the AR minimum in both the *x*-*z* and *y*-*z* planes are shown in Fig. 10(a) and (b), respectively. The measured gain is around 5.2 dBi, which is ∼0.7 dB lower than the simulation prediction. The simulated and measured angular dependence of the AR at the frequency where the AR is minimum in both the *x*-*z* and *y*-*z* planes are reported in Fig. 10(c) and (d). It can be observed that the AR of the fabricated prototype is smaller than 3 dB in the majority of the angular range covered by $-90° \leq \theta \leq 90°$. This result indicates that a good degree of circular polarization is achieved within a wide field-of-view, which would ensure a robust wireless link between the wearable antenna and a remote off-body receiver.

As a benchmark for comparison, an antenna with the same geometry but different dimensions was also designed targeting the 2.4 GHz ISM band and implemented using conventional printed circuit board (PCB) materials. Specifically, Rogers RO3003 ($\varepsilon_r = 3$ and $\tan\delta = 0.0013$) and copper were used as the substrate and conducting materials, respectively. This antenna has the same footprint and thickness as the flexible antenna realized using the PDMS and AgNW composite material system, but it is rigid. Fig. 11(a) and (b) show the simulated and measured S_{11} and broadside AR of the fabricated prototype [see the inset of Fig. 11(a)]. The measured results exhibit a good correspondence with the simulation predictions. The measured S_{11} is smaller than -10 dB from 2.35 to 2.61 GHz, which has a slightly broader bandwidth than the simulated result. The measured AR < 3 dB bandwidth is 67 MHz, centered at 2.46 GHz, which exhibits a shift of less than 1% compared to simulations. The measured antenna gain is about 6.1 dBi, while the simulated value is 7.0 dBi. The simulated radiation efficiency of this antenna is around 95% in the targeted band, due to the lower loss of the constitutive materials. In all, the flexible CP antenna implemented using the PDMS and AgNW composite shows

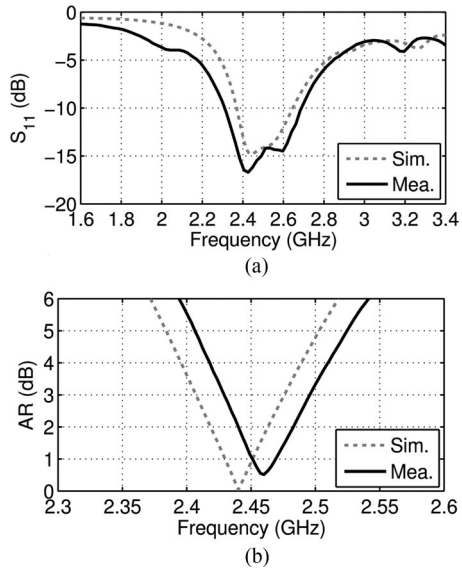

Fig. 9. Simulated and measured (a) S_{11} and (b) broadside AR of the antenna implemented using a composite of PDMS and AgNWs.

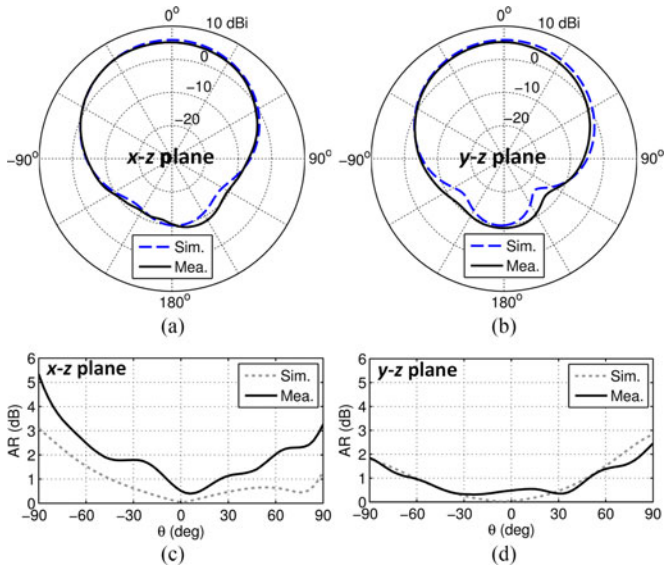

Fig. 10. Simulated and measured gain patterns of the total radiated power in the (a) *x*-*z* and (b) *y*-*z* planes. Simulated and measured angular dependence of AR in the (c) *x*-*z* plane and (d) *y*-*z* plane.

similar performance to its rigid PCB counterpart, with a gain degradation of only ∼0.9 dB due to material losses. However, the flexibility, lighter weight, and robustness of the proposed antenna represent key advantages for wearable applications.

IV. Comparison With a CP Patch Antenna

In order to appreciate the advantages of employing an AAG structure in the proposed antenna, its performance metric was compared to that of a conventional CP patch antenna which has the same footprint and thickness and is comprised by the same PDMS and AgNW composite. As the inset of Fig. 12(a) shows, the CP antenna is a microstrip fed square patch radiator with a

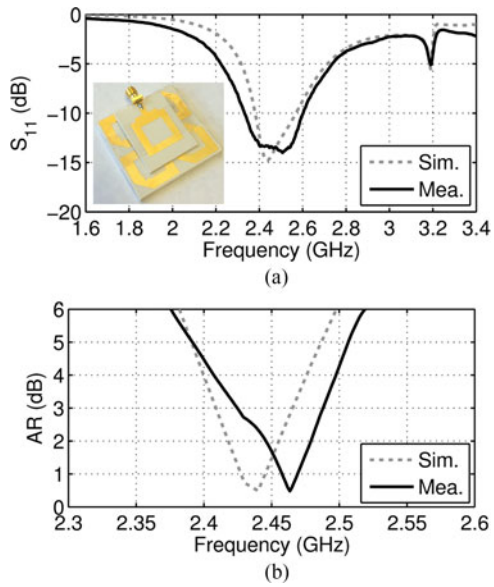

Fig. 11. Simulated and measured (a) S_{11} and (b) broadside AR of the antenna implemented using conventional PCB substrate material and copper. The inset shows a photograph of the antenna prototype.

pair of corners chamfered. Since the antenna needs to be conformal to the surfaces of different parts of a human body for wearable applications, both antennas are bent in free space with a certain radius of curvature, denoted as $R_{\rm a}$. Three typical values, including $R_{\rm a} = 100$, 75, and 50 mm, were considered, corresponding to the cases where the designed antenna was mounted on the chest, upper arm, and wrist, respectively. As displayed in Fig. 12(a), the bending has almost no effect on the S_{11} of the proposed antenna, while the CP patch antenna experiences a significant frequency shift and bandwidth broadening [28]. Importantly, for the AR < 3 bandwidth, the proposed antenna has a frequency shift of less than 15 MHz. In contrast, the AR < 3 bandwidth of the CP patch antenna experiences a blueshift of more than 90 MHz. This implies that the proposed antenna can be used at almost any location on a human body, which is not the case for the CP patch antenna. The RHCP gain value of the proposed antenna is about 1 dB higher than the CP patch antenna, as shown in Fig. 12(c). By bending the antenna from flat to having a radius of curvature of 50 mm, the gain drop in the targeted band is less than 0.3 dB for the proposed antenna, while more than 1.5 dB of gain reduction can be seen for the CP patch antenna due to its frequency shift. As revealed by Fig. 12(d), the bending also greatly reduces the FBTR ratio of the CP patch antenna, resulting in more radiated power into the half-space below the antenna, *i.e.* towards the human body. In contrast, the FBTR ratio for the proposed antenna is almost unaltered by structural deformation. The much more robust performance of the proposed antenna compared to the CP patch antenna lies in the fact that the former has four resonators, *i.e.* the MLRs of the AAG, covering the aperture rather than a single resonant cavity which is larger in size. Under structural deformation, the distributed MLRs of the proposed antenna experience less bending compared to the single resonant cavity with a larger size, thus resulting in a smaller frequency shift and quality factor reduction.

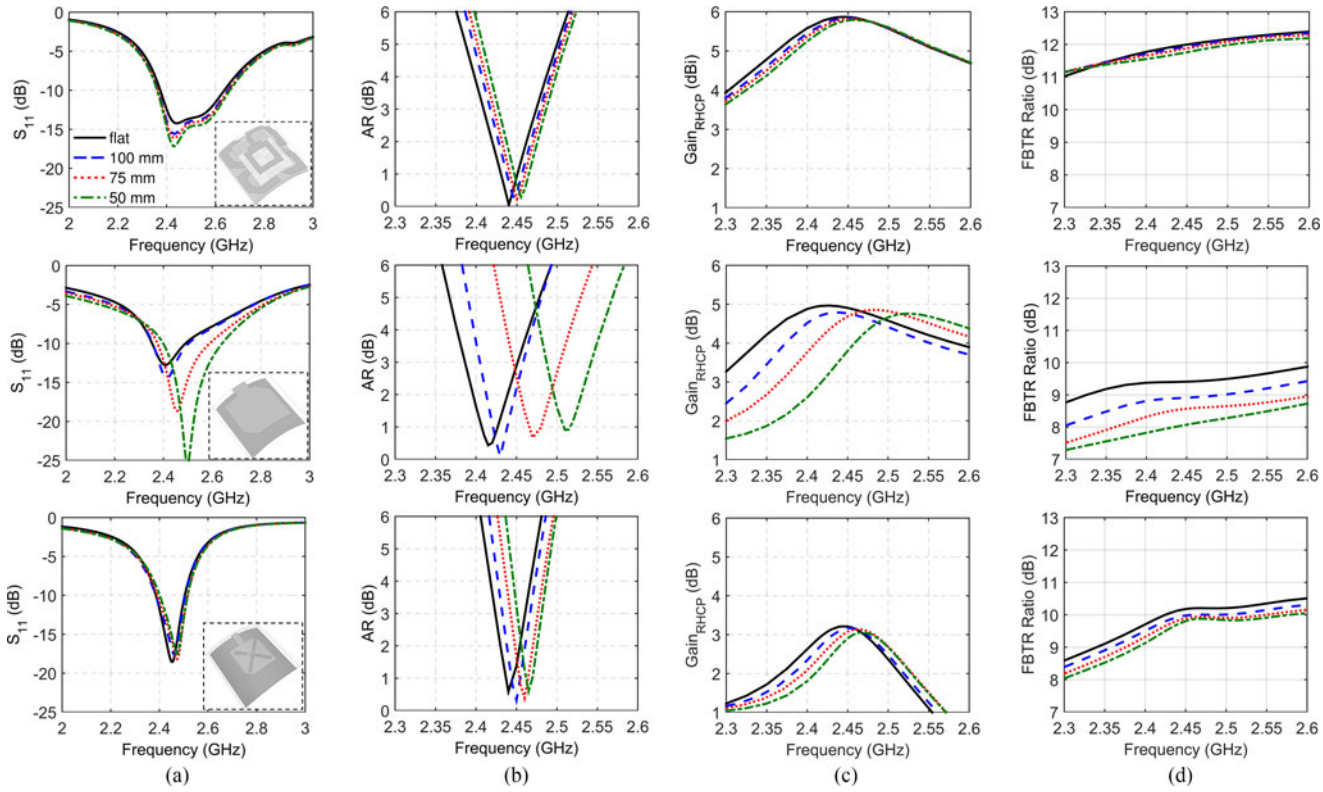

Fig. 12. Simulated (a) S_{11}, (b) Broadside AR, (c) RHCP gain, and (d) FBTR ratio of the proposed CP wearable antenna (top), a conventional CP patch antenna (middle), and a miniaturized slot-loaded CP patch antenna (bottom) with various radii of curvature.

TABLE I
PROPERTY COMPARISON AMONG DIFFERENT CIRCULARLY POLARIZED WEARABLE ANTENNAS

	Overall Footprint	Profile	$S_{11} < -10$ dB Bandwidth	AR <3 dB Bandwidth	Gain (dBi)/Rad. Eff.	HPBW/ARBW	S_{11} Shift Under Bending[a]	AR Shift Under Bending[a]	Materials (Substrate/Conductor)
[26][b]	$0.4\,\lambda_0^2$	$0.08\,\lambda_0$	44%	23%	2.5/35%	~75°/~112°	~150 MHz	~150 MHz	Felt/Flectron
[27]	$0.66\,\lambda_0^2$	$0.03\,\lambda_0$	8.9%	2.18%	6.03/62%	~69°/NA	$<$20 MHz	NA	Foam/Shieldit Super & Fectron
[28]	$0.95\,\lambda_0^2$	$0.03\,\lambda_0$	12.8%	2.96%	4.4/34.7%	~74°/~43°	~98 MHz	~90 MHz	Felt/Conductive Fabric
[29]	$0.2\,\lambda_0^2$	$0.045\,\lambda_0$	4.5%	2.4%	3.5/58%	~88°/~103°	NA	NA	PCB/Copper
[30]	$0.28\,\lambda_0^2$	$0.07\,\lambda_0$	12.5%	12.5%	5.2/76%	~83°/~85°	NA	NA	PCB/Copper
[31]	$0.27\,\lambda_0^2$	NA	5.4%	1.23%	6.2/70%	~69°/~151°	~ 20 MHz	~ 15 MHz	Textile/Copper Plated Fabric
[32][c]	$0.2\,\lambda_0^2$	$0.013\,\lambda_0$	4.1%	1.25%	5.7/NA	~90°/NA	NA	NA	Denim/NA
[33]	$0.54\,\lambda_0^2$	$0.012\,\lambda_0$	6.4%	1.63%	2.25/NA	~90°/~86°	NA	NA	Denim/Copper
This work	$0.17\,\lambda_0^2$	$0.045\,\lambda_0$	15.9%	2.72%	5.2/79%	~89°/~171°	~ 0 MHz	$<$15 MHz	PDMS/AgNW

[a]The bending radius is 50 mm.
[b]The corresponding antenna has bi-directional radiation while all the others have unidirectional radiation.
[c]Only simulated results are available.

In addition, the proposed antenna operates in between the resonant modes of the MLRs [see Fig. 2(b)], while the CP band is located very close to the resonance of the patch cavity. Hence, the proposed antenna has a lower overall absorption loss than the CP patch antenna, which leads to a higher radiation efficiency. A further comparison was carried out by considering a miniaturized CP patch antenna with a crossed slot cut in the center (see the left column of Fig. 12). The patch has a similar size to that of a single MLR, while the footprint and thickness of the entire antenna structure are kept the same. Indeed, the miniaturized cavity greatly improves the performance stability reducing the frequency shift down to only 25 MHz. However, this amount of shift is still larger than that of the proposed antenna. In addition, due to the increased quality factor of the antenna and the fact that the entire aperture is not efficiently utilized, such a robust behavior is achieved at the expense of an inferior overall performance including a narrower S_{11} and AR bandwidths, a lower gain, and a smaller FBTR ratio, which corroborates results reported in the literature [31]–[33].

Table I compares the properties of the proposed antenna with those of the other previously reported CP wearable antennas. It can be seen that the demonstrated antenna possesses the small-

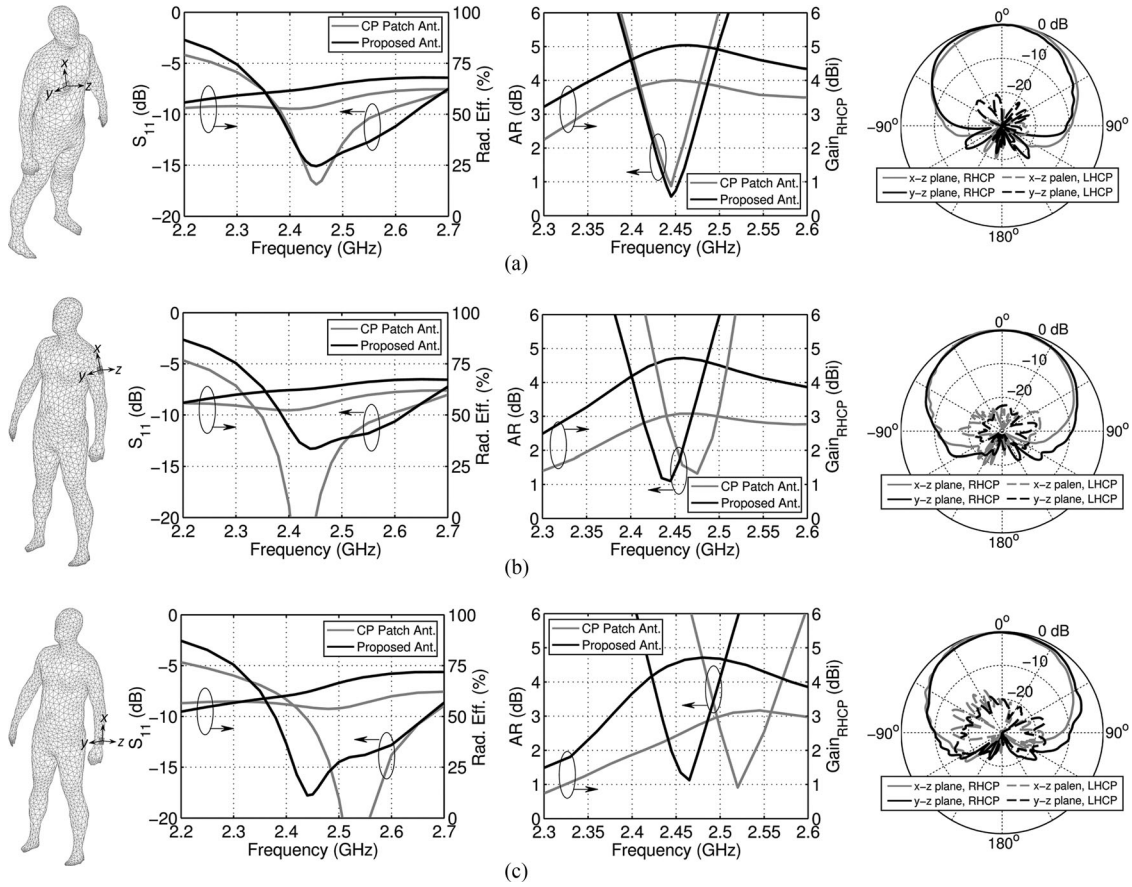

Fig. 13. Simulated S_{11}, radiation efficiency, broadside AR, RHCP gain of both the proposed antenna and the conventional CP patch antenna, as well as simulated normalized LHCP and RHCP radiation patterns corresponding to the frequency of AR minimum in both the *x*-*z* and *y*-*z* planes of the proposed antenna mounted on the (a) chest, (b) arm, and (c) wrist of a human body model.

est footprint, largest impedance bandwidth, highest radiation efficiency, widest AR beamwidth, and most robust performance under structural deformation.

V. On-body Simulations and Measurements

To evaluate the suitability of the proposed antenna in wearable applications to enable effective off-body communications, its performance is investigated and compared to that of a conventional CP patch antenna. In this study, three different mounting positions for the antennas were considered (*i.e.*, on the chest, upper arm, and wrist of a human body model, corresponding to $R_a = 100$, 75, and 50 mm, respectively).

A. Impact of the Human Body on Antenna Performance

The impact of the human body on the input impedance and the radiation properties of both a conventional CP patch antenna and the proposed antenna were studied. A homogenous full-scale human body model was employed which had a height of 174 cm and a chest width of 46 cm [57]. Its homogeneous permittivity was chosen to be 2/3 of the permittivity of muscle, which represents a reasonable approximation as proven in the literature [1], [4], [58]. In the HFSS simulation domain, the human body model was assigned as an integral equation (IE) region, which was solved by the method of moments, while the CP patch antenna and the proposed antenna were assigned as finite element regions. Such a homogeneous model provides a numerically economical means to generating a fairly accurate evaluation of both the impedance and radiation properties of wearable antennas, but not the SAR values [21], [29], [30].

As shown in Fig. 13(a)–(c), the proposed antenna was placed at three different locations on the human body model, including the chest, the upper arm, and the wrist, with an antenna-to-body distance of approximately 4 mm. Owing to the employed AAG, which greatly reduces the back radiation, the human body in close proximity does not have a significant impact on the electromagnetic properties of the proposed antenna. Moreover, due to its robust properties with respect to structural deformation, the performance of the proposed antenna is expected to be well maintained when it is mounted conformally on different locations of a human body. Indeed, the S_{11}, radiation efficiency, broadside AR, and gain remain almost the same when compared with those of the antenna in free space. The resonances in the S_{11} remain at the same frequency for all three cases. The broadside gain profiles are also well maintained with a peak gain of 5.1, 4.9, and 4.8 dBi for the on-chest, on-upper-arm, and on-wrist cases, respectively. The simulated radiation efficiency of the antenna in the targeted band is around 68%, which is $\sim$10% lower than that of the antenna in free space. This slight drop indicates that there is only a minor impact on the

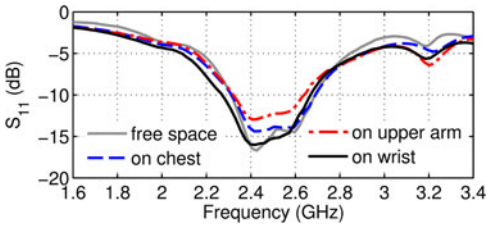

Fig. 14. Measured S_{11} of the CP wearable antenna prototype mounted on different parts of a human body.

radiation efficiency of the antenna when it is located in close proximity to human tissue, due to the employed AAG structure. The broadside ARs are all below 3 dB in the majority of the targeted band, with a frequency shift of only 20 MHz when moving the antenna from the chest to the wrist. This frequency shift is partially due to the bending of the antenna, as previously discussed, which implies that the impact of the human body has an almost negligible effect on the AR of the antenna. The simulated normalized LHCP and RHCP radiation patterns of the proposed antenna in both the *x*-*z* and *y*-*z* planes at the frequency of AR minimum for all three cases are also displayed in Fig. 13. It can be seen that the majority of the energy is directed into the hemisphere away from the human body. The HPBW in the *x*-*z*/*y*-*z* planes are 88°/90°, 89°/94°, and 98°/101° for the on-chest, on-upper-arm, and on-wrist cases, respectively. Slight differences exist between the radiation patterns of the antenna in free space and when it is mounted on-body. Particularly, minor pattern asymmetry and squinting can be observed, primarily due to the human body shadowing effect. The multiple lobes of cross-polarization in the half space in front of the antenna are caused by the fact that the LHCP back radiation is converted into RHCP waves, upon reflecting from the human body surface beneath the antenna, which interferes with the RHCP waves directly radiated from the antenna. Nevertheless, the radiation patterns exhibit high cross polarization discrimination within a wide angular range. Such simultaneous wide angular power and circular polarization coverage indicates that stable wireless links could be achieved for off-body communications. Experiments were performed with the antenna when placed on the three different parts of a human body in order to validate its predicted robust impedance property. As shown in Fig. 14, it can be seen that the measured S_{11} of the antenna prototype on the chest, upper arm, and wrist are almost identical to that of the antenna in free space, confirming the very small loading effect due to the human body.

As a comparison, full-wave simulations of the conventional CP patch antenna mounted on the three different locations of the human body model were also performed. It can be seen from Fig. 13 that the simulated radiation efficiency is only about 55% in the targeted band. In addition, significant frequency shifts occur in both the S_{11} and the AR among the three difference cases, partially due to the bending of the antenna structure. Moreover, the gain is reduced by around 1.8 dB as compared to the value of the CP patch antenna in free space for all three cases. This indicates that the CP patch antenna is not immune to the loading

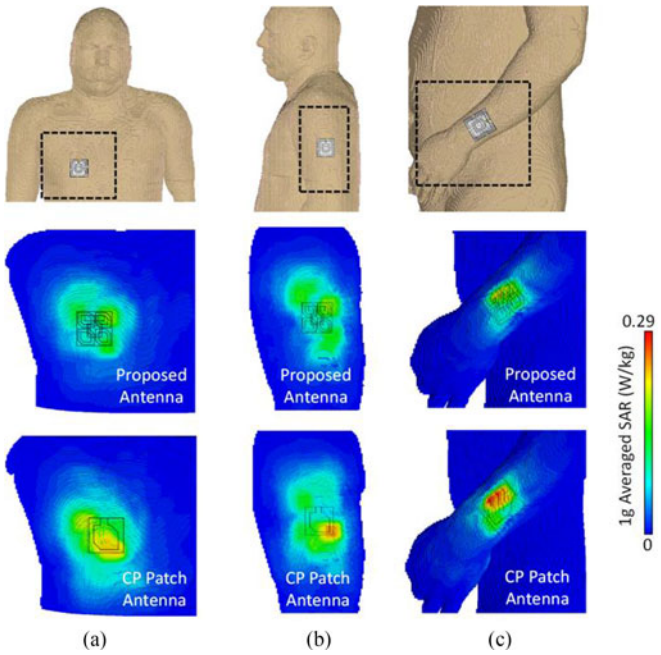

Fig. 15. Simulated 1 g averaged SAR values of both the proposed antenna and the conventional CP patch antenna mounted on (a) the chest, (b) the upper arm, and (c) the wrist of the HUGO human body model in CST MWS at 2.44 GHz.

effects when placed in close proximity to a human body, demonstrating that it is interfior to the proposed antenna for wearable applications. It should be noted that, when directly placing the top loop monopole antenna in close proximity to the human body surface without the AAG shielding, the radiation efficiency will be significantly reduced to just a few percent, which is attributed to its bi-directional radiation pattern [25], [26].

B. SAR Simulations

To evaluate the SAR, which quantifies the effect of the antenna on the human body, a numerical 3D volumetric anatomical HUGO human body model produced by the National Library of Medicine [59] was incorporated into the CST microwave studio (MWS) software package. This approach allowed for accurate calculation of the SAR values in the near-field, which contains 40 different types of tissues at a resolution of $2 \times 2 \times 2$ mm mesh size.

As shown in the top row of Fig. 15(a)–(c), the proposed antenna was placed at three different positions on the HUGO human body, including the chest, the upper arm, and the wrist, respectively. The distance between the antenna and the human body model surfaces was set to be around 4 mm. As a benchmark, a power of 100 mW accepted by the antenna was chosen to evaluate the SAR performance. To reduce the simulation time, only a portion of the chest or arm with a sectional area of larger than 10 times that of the antenna size was used since the SAR is a near-field effect. The middle row of Fig. 15(a)–(c) respectively show the simulated 1 g averaged SAR values due to the proposed antenna for the three cases, while the bottom row displays the corresponding SAR distribution resulting from the conventional CP patch antenna. For the conventional CP patch

antenna, the peak 1 g averaged SAR varies from 0.22 to 0.29 W/kg. For the proposed antenna, however, it can be observed that, for all three cases, the peak 1 g averaged SAR value ranges from 0.13 to 0.18 W/kg. This indicates that the maximum allowed accepted power for the proposed antenna is about 65% higher than that for the CP patch antenna, thereby leading to a larger maximum communication distance of about 30%. These values are not only well below the 1.6 W/kg specification provided by the Federal Communication Commission (FCC) [60], but also much smaller than those of the conventional CP patch antenna.

VI. Conclusions

In summary, we have reported a methodology to design compact and robust CP wearable antennas using an AAG with only 2 by 2 unit cells. A composite of PDMS and AgNWs was employed to implement the antenna prototype, thereby achieving a fully planar and highly flexible module. Experimental results were found to be in strong agreement with the simulation predictions, thus confirming the proposed design. The reported antenna was shown to have a robust performance against structural deformation and human body loading, which is far superior to a conventional CP patch antenna. Moreover, the proposed antenna exhibits small SAR values in several examined wearable scenarios. The demonstrated compact, flexible, and highly efficient CP antenna is expected to find potential applications in various advanced wearable devices for off-body communications.

References

[1] P. S. Hall and Y. Hao, *Antennas and Propagation for Body-Centric Wireless Communications*. Norwood, MA, USA: Artech House, 2012.

[2] G. Z. Yang, *Body Sensor Networks*. Berlin, Germany: Springer, 2006.

[3] C. S. Nikita, *Handbook of Biomedical Telemetry*. Hoboken, NJ, USA: Wiley-IEEE Press, 2014.

[4] D. H. Werner and Z. H. Jiang, *Electromagnetics of Body Area Networks: Antennas, Propagation, and RF Systems*. Hoboken, NJ, USA: Wiley/IEEE Press, 2016.

[5] P. S. Hall *et al.*, "Antennas and propagation for on-body communication systems," *IEEE Antennas Propag. Mag.*, vol. 49, no. 3, pp. 41–58, Jun. 2007.

[6] N. H. M. Rais, P. J. Soh, F. Malek, S. Ahmad, N. Hashim, and P. S. Hall, "A review of wearable antenna," in *Proc. Loughborough Antennas Propag. Conf.*, 2009, pp. 225–228.

[7] R. Moro, S. Agneessens, H. Rogier, A. Dierck, and M. Bozzi, "Textile microwave components in substrate integrated waveguide technology," *IEEE Trans. Microw. Theory Tech.*, vol. 63, no. 2, pp. 422–432, Feb. 2015.

[8] S. Yao and Y. Zhu, "Nanomaterial-enabled stretchable conductors: strategies, materials and devices," *Adv. Mater.*, vol. 27, no. 9, pp. 1480–1511, Jan. 2015.

[9] C. A. Winterhalter *et al.*, "Development of electronic textiles to support networks, communications, and medical applications in future U.S. Military protective clothing systems," *IEEE Trans. Inf. Technol. Biomed.*, vol. 9, no. 3, pp. 402–406, Sep. 2005.

[10] M. Klemm and G. Troester, "Textile UWB antennas for wireless body area networks," *IEEE Trans. Antennas Propag.*, vol. 54, no. 11, pp. 3192–3197, Nov. 2006.

[11] S. Sankaralingam and B. Gupta, "Determination of dielectric constant of fabric materials and their use as substrates for design and development of antennas for wearable applications," *IEEE Trans. Instrum. Meas.*, vol. 59, no. 12, pp. 3122–3130, Dec. 2010.

[12] P. J. Soh, G. A. E. Vandenbosch, S. L. Ooi, and M. R. N. Husna, "Wearable dual-band Sierpinski fractal PIFA using conductive fabric," *Electron. Lett.*, vol. 47, no. 6, pp. 365–367, Mar. 2011.

[13] M. N. Suma, P. C. Bybi, and P. Mohanan, "A wideband printed monopole antenna for 2.45 GHz WLAN applications," *Microw. Opt. Technol. Lett.*, vol. 48, no. 5, pp. 871–873, May 2006.

[14] A. Alomainy *et al.*, "Statistical analysis and performance evaluation for on-body radio propagation with microstrip patch antennas," *IEEE Trans. Antennas Propag.*, vol. 55, no. 1, pp. 245–248, Jan. 2007.

[15] N. Haga, K. Saito, M. Takahashi, and K. Ito, "Characteristics of cavity slot antenna for body-area networks," *IEEE Trans. Antennas Propag.*, vol. 57, no. 4, pp. 837–843, Apr. 2009.

[16] S. Agneessens and H. Rogier, "Compact half diamond dual-band textile HMSIW on-body antenna," *IEEE Trans. Antennas Propag.*, vol. 62, no. 5, pp. 2374–2381, May 2014.

[17] S. Agneessens, S. Lemey, T. Vervust, and H. Rogier, "Wearable, small, and robust: the circular quarter-mode textile antenna," *IEEE Antennas Wireless Propag. Lett.*, vol. 14, pp. 1482–1485, Jan. 2015.

[18] S. Yan, P. J. Soh, and G. A. E. Vandenbosch, "Dual-band textile MIMO antenna based on substrate-integrated waveguide (SIW) technology," *IEEE Trans. Antennas Propag.*, vol. 63, no. 11, pp. 4640–4647, Nov. 2015.

[19] P. J. Soh, G. A. E. Vandenbosch, S. L. Ooi, and N. H. M. Rais, "Design of a broadband all-textile slotted PIFA," *IEEE Trans. Antennas Propag.*, vol. 60, no. 1, pp. 379–384, Jan. 2012.

[20] W. El Hajj, C. Person, and J. Wiart, "A novel investigation of a broadband integrated inverted-F antenna design; application for wearable antenna," *IEEE Trans. Antennas Propag.*, vol. 62, no. 7, pp. 3843–3846, Jul. 2014.

[21] Z. Wang, L. Z. Lee, D. Psychoudakis, and J. L. Volakis, "Embroidered multiband body-worn antenna for GSM/PCS/WLAN communications," *IEEE Trans. Antennas Propag.*, vol. 62, no. 6, pp. 3321–3329, Jun. 2014.

[22] S. Zhu and R. Langley, "Dual-band wearable textile antenna on an EBG substrate," *IEEE Trans. Antennas Propag.*, vol. 57, no. 4, pp. 926–935, Apr. 2009.

[23] H. R. Raad, A. I. Abbosh, H. M. Al-Rizzo, and D. G. Rucker, "Flexible and compact AMC based antenna for telemedicine applications," *IEEE Trans. Antennas Propag.*, vol. 61, no. 2, pp. 524–531, Feb. 2013.

[24] S. Yan, P. J. Soh, and G. A. E. Vandenbosch, "Low-profile dual-band textile antenna with artificial magnetic conductor plane," *IEEE Trans. Antennas Propag.*, vol. 62, no. 12, pp. 6587–6490, Dec. 2014.

[25] Z. H. Jiang, D. E. Brocker, P. E. Sieber, and D. H. Werner, "A compact, low-profile metasurface-enabled antenna for wearable medical body-area network devices," *IEEE Trans. Antennas Propag.*, vol. 62, no. 8, pp. 4021–4030, Aug. 2014.

[26] K. W. Lui, O. H. Murphy, and C. Toumazou, "A wearable wideband circularly polarized textile antenna for effective power transmission on a wireless-powered sensor platform," *IEEE Trans. Antennas Propag.*, vol. 61, no. 7, pp. 3873–3876, Jul. 2013.

[27] C. Hertleer, H. Rogier, L. Vallozzi, and L. Van Langenhove, "A textile antenna for off-body communication integrated into protective clothing for firefighters," *IEEE Trans. Antennas Propag.*, vol. 57, no. 4, pp. 919–925, Apr. 2009.

[28] I. Locher, M. Klemm, T. Kirstein, and G. Tröster, "Design and characterization of purely textile patch antennas," *IEEE Trans. Adv. Packag.*, vol. 29, no. 4, pp. 777–788, Nov. 2006.

[29] Z. H. Jiang, M. D. Gregory, and D. H. Werner, "Design and experimental investigation of a compact circularly polarized integrated filtering antenna for wearable biotelemetric devices," *IEEE Trans. Biomed. Circuits Syst.*, vol. 10, no. 2, pp. 328–338, Apr. 2016.

[30] Z. H. Jiang and D. H. Werner, "A compact, wideband circularly polarized co-designed filtering antenna and its application for wearable devices with low SAR," *IEEE Trans. Antennas Propag.*, vol. 63, no. 9, pp. 3808–3818, Sep. 2015.

[31] E. K. Kaivanto, M. Berg, E. Salonen, and P. de Maagt, "Wearable circularly polarized antenna for personal satellite communication and navigation," *IEEE Trans. Antennas Propag.*, vol. 59, no. 12, pp. 4490–4496, Dec. 2011.

[32] M. F. Ismail, M. K. A. Rahim, E. I. S. Saadon, and M. S. Mohd, "Compact circularly polarized textile antenna," in *Proc. 2014 IEEE Symp. Wireless Tech. Appl.*, Oct. 2014, pp. 134–136.

[33] M. Rizwan, Y. Rahmat-Samii, and L. Ukkonen, "Circularly polarized textile antenna for 2.45 GHz," in Proc. *2015 IEEE MTT-S 2015 Int. Microw. Workshop Series RF Wireless Technol. Biomed. Healthcare Appl.*, Dec. 2015, pp. 21–22.

[34] G. J. Hayes, J.-H. So, A. Qusba, M. D. Dickey, and G. Lazzi, "Flexible liquid metal alloy (EGaIn) microstrip patch antenna," *IEEE Trans. Antennas Propag.*, vol. 60, no. 5, pp. 2151–2156, May 2012.

[35] C. Myers, H. Huang, and Y. Zhu, "Wearable silver nanowire dry electrodes for electrophysiological sensing," *RSC Adv.*, vol. 5, no. 15, pp. 11627–11632, Jan. 2015.

[36] J. Krupka, W. Gwarek, N. Kwietniewski, and J. G. Hartnett, "Measurements of planar metal–dielectric structures using split-post dielectric resonators," *IEEE Trans. Microw. Theory Tech.*, vol. 58, no. 12, pp. 3511–3518, Dec. 2010.
[37] F. Xu and Y. Zhu, "Highly conductive and stretchable silver nanowire conductors," *Adv. Mater.*, vol. 24, no. 37, pp. 5117–5122, Sep. 2012.
[38] L. Li, Z. Yu, W. Hu, C.-H. Chang, Q. Chen, and Q. Pei, "Efficient flexible phosphorescent polymer light-emitting diodes based on silver nanowire-polymer composite electrode," *Adv. Mater.*, vol. 23, no. 46, pp. 5563–5567, Dec. 2011.
[39] D.-S. Leem, A. Edwards, M. Faist, J. Nelson, D. D. C. Bradley, and J. C. de Mello, "Efficient organic solar cells with solution-processed silver nanowire electrodes," *Adv. Mater.*, vol. 23, no. 38, pp. 4371–4375, Oct. 2011.
[40] J. Lee, P. Lee, H. Lee, D. Lee, S. S. Lee, and S. H. Ko, "Very long Ag nanowire synthesis and its application in a highly transparent, conductive and flexible metal electrode touch panel," *Nanoscale*, vol. 4, no. 20, pp. 6408–6414, Dec. 2012.
[41] Z. Cui, F. R. Poblete, G. Cheng, S. Yao, X. Jiang, and Y. Zhu, "Design and operation of silver nanowire based flexible and stretchable touch sensors," *J. Mater. Res.*, vol. 30, no. 1, pp. 79–85, Jan. 2015.
[42] S. Yao and Y. Zhu, "Wearable multifunctional sensors using printed stretchable conductors made of silver nanowires," *Nanoscale*, vol. 6, no. 4, pp. 2345–2352, Feb. 2014.
[43] L. Song, A. C. Myers, J. J. Adams, and Y. Zhu, "Stretchable and reversibly deformable radio frequency antennas based on silver nanowires," *ACS Appl. Mater. Int.*, vol. 6, no. 6, pp. 4248–4253, Mar. 2014.
[44] T. Inui, H. Koga, M. Nogi, N. Komoda, and K. Suganuma, "A miniaturized flexible antenna printed on a high dielectric constant nanopaper composite," *Adv. Mater.*, vol. 27, no. 6, pp. 1112–1116, Feb. 2015.
[45] K. Agarwal, Y.-X. Guo, and B. Salam, "Wearable AMC backed near-endfire antenna for on-body communications on latex substrate," *IEEE Trans. Compon., Packag., Manuf. Technol.*, vol. 6, no. 3, pp. 346–358, Mar. 2016.
[46] K. Agarwal, Nasimuddin, and A. Alphones, "Unidirectional wideband circularly polarised aperture antennas backed with artificial magnetic conductor reflectors," *IET Microw. Antennas Propag.*, vol. 7, no. 5, pp. 338–346, Apr. 2013.
[47] A. Foroozesh and L. Shafai, "Investigation into the application of artificial magnetic conductors to bandwidth broadening, gain enhancement and beam shaping of low profile and conventional monopole antennas," *IEEE Trans. Antennas Propag.*, vol. 59, no. 1, pp. 4–20, Jan. 2011.
[48] L. J. Foged *et al.*, "Miniaturized array antenna using artificial magnetic materials for satellite-based AIS system," *IEEE Trans. Antennas Propag.*, vol. 63, no. 4, pp. 1276–1287, Apr. 2015.
[49] A. Foroozesh and L. Shafai, "Effects of artificial magnetic conductors in the design of low-profile high-gain planar antennas with high-permittivity dielectric superstrate," *IEEE Antennas Wireless Propag. Lett.*, vol. 8, pp. 10–13, Mar. 2009.
[50] B. S. Cook and A. Shamim, "Utilizing wideband AMC structures for high-gain inkjet-printed antennas on lossy paper substrate," *IEEE Antennas Wireless Propag. Lett.*, vol. 12, pp. 76–79, Mar. 2013.
[51] F. Yang and Y. Rahmat-Samii, "A low profile single dipole antenna radiating circularly polarized waves," *IEEE Trans. Antennas Propag.*, vol. 53, no. 9, pp. 3083–3086, Sep. 2005.
[52] T. Nakamura and T. Fukusako, "Broadband design of circularly polarized microstrip patch antenna using artificial ground structure with rectangular unit cells," *IEEE Trans. Antennas Propag.*, vol. 59, no. 6, pp. 2103–2110, Jun. 2011.
[53] [Online]. Available: http://www.ansys.com/Products/Electronics/ANSYSHFSS.
[54] T. Yue, Z. H. Jiang, and D. H. Werner, "Compact, wideband antennas enabled by interdigitated capacitor loaded metasurfaces," *IEEE Trans. Antennas Propag.*, vol. 64, no. 5, pp. 1595–1606, May 2016.
[55] I. J. Bahl and P. Bhartia, *Microstrip Antennas*. Dedham, MA, USA: Artech House, 1982.
[56] S. Noghanian and L. Shafai, "Control of microstrip antenna radiation characteristics by ground plane size and shape," *IEE Proc. Microw. Antennas Propag.*, vol. 145, no. 3, pp. 207–212, Jun. 1998.
[57] S. N. Makarov, G. M. Noetscher, and A. Nazarian, *Low-Frequency Electromagnetic Modeling for Electrical and Biological Systems Using MATLAB*. Hoboken, NJ, USA: Wiley, 2015.
[58] C. Furse, D. A. Christensen, and C. H. Durney, *Basic Introduction to Bioelectromagnetics*, 2nd ed. Boca Raton, FL, USA: CRC Press, 2009.
[59] Computer Simulation Technology (CST), Framingham, MA, USA, "HUGO human body model," 2014. [Online]. Available: https://www.cst.com/Applications/Article/HUGO+Human+Body+Model.
[60] IEEE Recommended Practice for Measurements and Computations of Radio Frequency Electromagnetic Fields with Respect to Human Exposure to Such Fields, 100 kHz–300 GHz, IEEE Std. C95.3-2002, 2002.

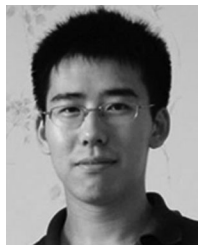

Zhi Hao Jiang (S'07–M'13) was born in Nanjing, China, in 1986. He received the B.S. degree in radio engineering from Southeast University, Nanjing, China, in 2008, and the Ph.D. degree in electrical engineering from The Pennsylvania State University, University Park, PA, USA, in 2013.

He is currently a Full Professor in the State Key Laboratory of Millimeter Waves, School of Information Science and Engineering, Southeast University. From August 2013 to July 2016, he was a Postdoc Fellow in the Computational Electromagnetics and Antennas Research Lab, Department of Electrical Engineering, The Pennsylvania State University. From July 2007 to August 2007, he was an Intern in the Base Station Antenna R&D, Andrew Telecommunication (China). He holds 5 US patents (2 granted, 3 pending) and 1 Chinese patent, has authored more than 80 papers in peer reviewed international journals and conference proceedings, as well as 7 book chapters. He has co-edited 1 book: *Electromagnetics of Body-area Networks: Antennas, Propagation, and RF Systems* (Wiley/IEEE Press, 2016). His research interests include antennas, transmit-arrays, impedance surfaces, microwave circuits, metamaterials, and nanophotonics. He received the Thousands of Young Talents presented by China government in 2016, the Honorable Mention in 2013 IEEE AP-S International Symposium on Antennas and Propagation Student Paper Contest, the 2012 A. J. Ferraro Outstanding Doctoral Research Award in Electromagnetics, the 2007 Microsoft Young Fellow awarded by Microsoft Research Asia, and the Meritorious Winner of the 2006 Interdisciplinary Contest in Modeling funded by National Security Agency and administrated by the Consortium for Mathematics and its Applications. He also serves as a Reviewer for *Nature Communications*, *Scientific Reports*, IEEE TRANSACTIONS ON ANTENNAS AND PROPAGATION, IEEE TRANSACTIONS ON BIOMEDICAL CIRCUITS AND SYSTEMS, IEEE ANTENNAS AND WIRELESS PROPAGATION LETTERS, IEEE MICROWAVE AND WIRELESS COMPONENT LETTERS, IEEE ANTENNAS AND PROPAGATION MAGAZINE, *Applied Physics Letters*, and so on.

Zheng Cui was born in Hebei province, China. He received his B.S. degrees in mechanical engineering from Hefei University of Technology in 2013. He is pursuing his Ph.D. degree in Dr. Yong Zhu's lab at Department of Mechanical and Aerospace Engineering, North Carolina State University. His research interest focuses on nanostructure-enabled stretchable electronics.

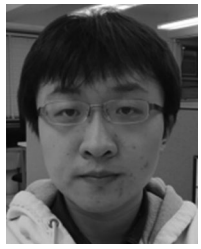

Taiwei Yue (S'14) was born in Wuhan, China, in 1991. He received the B.S. degree in physics from Nanjing University, Nanjing, China, in 2013. He is currently working toward the Ph.D. degree in the Computational Electromagnetics and Antennas Research Lab, Department of Electrical Engineering, The Pennsylvania State University, University Park, PA, USA.

His research interests include antennas engineering, RF/microwave circuits design, metamaterials, and plasmonics.

Yong Zhu received the B.S. degree in mechanics and mechanical engineering from the University of Science and Technology of China, Hefei, China, in 1999, and the M.S. and Ph.D. degrees in mechanical engineering from Northwestern University, Evanston, IL, USA, in 2001 and 2005, respectively. He was a Postdoctoral Fellow with the University of Texas at Austin before joining the North Carolina State University, Raleigh, NC, USA, in 2007. He is currently an Associate Professor of Mechanical and Aerospace Engineering and an Adjunct Professor of Materials Science and Engineering and Biomedical Engineering. He is an Author or Co-Author of four book chapters and more than 60 peer-reviewed journal papers. His research interests include mechanics of nanomaterials, micro/nano-electromechanical systems, and flexible/stretchable electronics.

Douglas H. Werner (F'05) received the B.S., M.S., and Ph.D. degrees in electrical engineering and the M.A. degree in mathematics from The Pennsylvania State University (Penn State), University Park, PA, USA, in 1983, 1985, 1989, and 1986, respectively.

He holds the John L. and Genevieve H. McCain Chair Professorship in The Pennsylvania State University Department of Electrical Engineering, University Park, PA, USA. He is the Director of the Computational Electromagnetics and Antennas Research Lab (http://cearl.ee.psu.edu/) as well as a member of the Communications and Space Sciences Lab. He is also a Faculty Member of the Materials Research Institute, Penn State. He holds 13 patents, has published more than 725 technical papers and proceedings articles, and is the Author of 20 book chapters with several additional chapters currently in preparation. He has published several books including *Frontiers in Electromagnetics* (Piscataway, NJ: IEEE Press, 2000), *Genetic Algorithms in Electromagnetics* (Hoboken, NJ: Wiley/IEEE, 2007), *Transformation Electromagnetics and Metamaterials: Fundamental Principles and Applications* (London, UK: Springer, 2014), and *Electromagnetics of Body Area Networks: Antennas, Propagation, and RF Systems* (Hoboken, NJ: Wiley/IEEE, 2016). He has also contributed chapters for several books including *Electromagnetic Optimization by Genetic Algorithms* (New York: Wiley Interscience, 1999), *Soft Computing in Communications* (New York: Springer, 2004), *Antenna Engineering Handbook* (New York: McGraw-Hill, 2007), *Frontiers in Antennas: Next Generation Design and Engineering* (New York: McGraw-Hill, 2011), *Numerical Methods for Metamaterial Design* (New York: Springer, 2013), *Computational Electromagnetics* (New York: Springer, 2014), *Graphene Science Handbook: Nanostructure and Atomic Arrangement* (Abingdon, Oxfordshire, UK: CRC Press, 2016), *Handbook of Antenna Technologies* (New York: Springer, 2016), and *Transformation Wave Physics: Electromagnetics, Elastodynamics and Thermodynamics* (Boca Raton, FL: CRC Press, 2016). His research interests include computational electromagnetics, antenna theory and design, phased arrays (including ultra-wideband arrays), microwave devices, wireless and personal communication systems (including on-body networks), wearable and e-textile antennas, RFID tag antennas, conformal antennas, reconfigurable antennas, frequency selective surfaces, electromagnetic wave interactions with complex media, metamaterials, electromagnetic bandgap materials, zero and negative index materials, transformation optics, nanoscale electromagnetics (including nanoantennas), fractal and knot electrodynamics, and nature-inspired optimization techniques (genetic algorithms, clonal selection algorithms, particle swarm, wind driven optimization, and various other evolutionary programming schemes).

Dr. Werner received the 1993 Applied Computational Electromagnetics Society (ACES) Best Paper Award, a 1993 International Union of Radio Science (URSI) Young Scientist Award, the Pennsylvania State University Applied Research Laboratory Outstanding Publication Award in 1994, the inaugural *IEEE Antennas and Propagation Society Edward E. Altshuler Prize Paper Award* and the *Harold A. Wheeler Applications Prize Paper Award* in 2011 and 2014, respectively, the *2015 ACES Technical Achievement Award*, a College of Engineering PSES Outstanding Research Award and Outstanding Teaching Award in March 2000 and March 2002, respectively, an IEEE Central Pennsylvania Section Millennium Medal, and in March 2009, the PSES Premier Research Award. He was a Co-Author (with one of his graduate students) of a paper published in the *IEEE Transactions on Antennas and Propagation* which received the 2006 R. W. P. King Award. He is a former Associate Editor of *Radio Science*, a former Editor of the *IEEE Antennas and Propagation Magazine*, an Associate Editor of the *Nature* subjournal *Scientific Reports*, a member of URSI Commissions B and G, Eta Kappa Nu, Tau Beta Pi and Sigma Xi. He is a Fellow of the IET (formerly IEE) and the ACES.